Magnetic anisotropy and low-energy spin waves in the Dzyaloshinskii-Moriya spiral magnet $Ba_2CuGe_2O_7$

A. Zheludev, S. Maslov, and G. Shirane
Brookhaven National Laboratory, Upton, New York 11973-5000

I. Tsukada, T. Masuda, and K. Uchinokura
Department of Applied Physics, The University of Tokyo, 7-3-1 Hongo, Bunkyo-ku, Tokyo 113-8656, Japan

I. Zaliznyak* and R. Erwin
National Institute of Standards and Technology Center for Neutron Research, National Institute of Standards and Technology, Gaithersburg, Maryland 20899

L. P. Regnault
Département de Recherche Fondamentale sur la Matière Condensée/Laboratoire de Magnétisme et Diffraction Neutronique, Centre d'Études Nucléaires de Grenoble, 17 rue des Martyrs, 38054 Grenoble Cedex, France

(Received 7 October 1998)

Neutron-diffraction and inelastic-scattering experiments are used to investigate in detail the field dependence of the magnetic structure and low-energy spin-wave spectrum of the Dzyaloshinskii-Moriya helimagnet $Ba_2CuGe_2O_7$. The results suggest that the previously proposed model for the magnetism of this compound (an ideal sinusoidal spin spiral, stabilized by isotropic exchange and Dzyaloshinskii-Moriya interactions) needs to be refined. Both recent and previously published data can be quantitatively explained by taking into account the Kaplan-Shekhtman-Entin-Wohlman-Aharony term, a special magnetic anisotropy term that was predicted to always accompany Dzyaloshinskii-Moriya interactions in insulators. [S0163-1829(99)01017-6]

I. INTRODUCTION

The recently discovered spiral magnet $Ba_2CuGe_2O_7$ is one of many materials known to have incommensurate magnetic structures.[1,2] A fortunate combination of properties, however, make $Ba_2CuGe_2O_7$ a particularly useful model system for both experimental and theoretical studies of incommensurate magnetism: (1) Unlike the extensively studied rare-earth compounds,[3] $Ba_2CuGe_2O_7$ is an insulator, and thus can be conveniently described in terms of localized spins. (2) Helimagnetism in $Ba_2CuGe_2O_7$ is caused by the somewhat exotic Dzyaloshinskii-Moriya off-diagonal exchange interactions[4,5] that involve only nearest-neighbor spins. This is in contrast with such well-known systems as MnO_2 (Ref. 6) and $NiBr_2$ (Refs. 7 and 8), where the magnetic incommensurability results from a competition between exchange interactions for different neighbor pairs (geometric frustration). (3) Compared to such classic Dzyaloshinskii-Moriya helimagnets as MnSi (Refs. 9 and 10) and FeGe (Ref. 11), $Ba_2CuGe_2O_7$ has a rather low (tetragonal) crystal symmetry. The result is a much richer field-temperature phase diagram. In particular, in $Ba_2CuGe_2O_7$ a magnetic field applied along the unique tetragonal axis induces a peculiar Dzyaloshinskii-type[12] incommensurate-to-commensurate transition.[13,14] Applying a magnetic field in the tetragonal plane does not change the length of the magnetic propagation vector, but leads to its reorientation.[15] (4) The spin arrangement in $Ba_2CuGe_2O_7$ is a perfect square lattice. This fact allowed us previously to describe the static properties of this remarkable system using a simple and elegant macroscopic free energy functional.[13–15] (5) Last but not least, the scale of energies and wave numbers that characterize magnetic interactions in $Ba_2CuGe_2O_7$ are very convenient for neutron-scattering measurements. Magnetic fields in which the most interesting magnetic phase transformations occur are also readily accessible using standard equipment.

As described in detail elsewhere (Refs. 1 and 14), the principal feature of $Ba_2CuGe_2O_7$ is a square-lattice arrangement of Cu^{2+} ions in the (a,b) plane of the tetragonal noncentric crystal structure (space group $P\bar{4}2_1m$, $a=8.466$ Å, $c=5.445$ Å). Nearest-neighbor in-plane antiferromagnetic exchange coupling [along the (1,1,0) direction] is by far the strongest magnetic interaction in the system ($J\approx 0.96$ meV per bond[16]). The interaction between Cu spins from adjacent planes is much weaker and ferromagnetic ($J_\perp \approx -0.026$ meV per bond). The magnetic structure can be described as an almost-antiferromagnetic spiral (Fig. 1, inset), with spins confined in the $(1,\bar{1},0)$ plane and the magnetic propagation vector $(1+\zeta,\zeta,0), \zeta\approx 0.0273$, (1,0,0) being the Néel point. It was previously demonstrated that the helimagnetic state is stabilized by nearest-neighbor Dzyaloshinskii-Moriya interactions that for two interacting spins $\boldsymbol{S}_1$ and $\boldsymbol{S}_2$ can be written as $(\boldsymbol{S}_1\times\boldsymbol{S}_2)\cdot\boldsymbol{D}^{(1,2)}$. For the Cu-Cu bond along the (1,1,0) direction (x axis) the Dzyaloshinskii vector $\boldsymbol{D}$ is pointing along $(1,\bar{1},0)$ (y axis), inducing a relative rotation of the interacting spins in the (x,z) plane (the z axis is chosen along the c axis of the crystal). The rotation angle ϕ (relative to a perfect antiparallel alignment) is related to the magnetic propagation vector by $\phi = 2\pi\zeta \approx 0.172$. Obviously, two types of domains, with

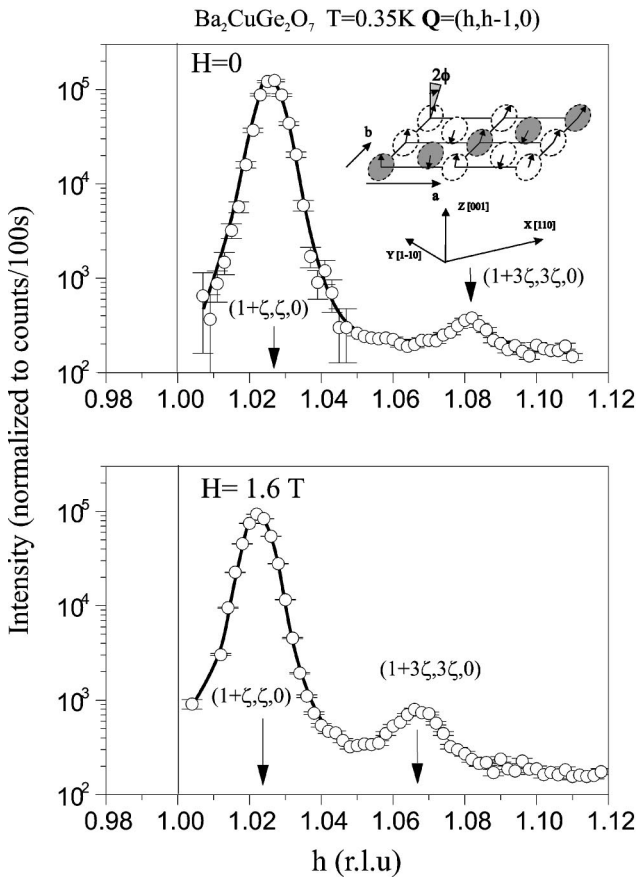

FIG. 1. Typical elastic scans along the (1,1,0) direction in the vicinity of the antiferromagnetic zone center (1,0,0), measured in $Ba_2CuGe_2O_7$ at $T=0.35$ K in zero field (top) and in a $H=1.6$ T magnetic field applied along the (0,0,1) direction (bottom). Note the logarithmic scale on the y axis. The solid lines are guides for the eye. The arrows show the positions of the principal magnetic Bragg reflections at $(1+\zeta,\zeta,0)$, characteristic of a spiral spin structure, and the third harmonic at $(1+3\zeta,3\zeta,0)$, a signature of a slight distortion of the helicoid. Inset: a schematic of the magnetic structure showing a single Cu plane in $Ba_2CuGe_2O_7$.

equivalent propagation vectors $(1+\zeta,\zeta,0)$ and $(1+\zeta,-\zeta,0)$ will always be present in a macroscopic sample.

By now, a large amount of experimental and theoretical work has been done on $Ba_2CuGe_2O_7$, mainly dealing with the phase transitions and static magnetic properties. Some important issues remain unresolved, however. For example, it was predicted that applying a magnetic field along the unique axis should give rise to a distortion of the ideal spiral structure.[13,14] This so-called soliton phase is characterized by the appearance of higher-order magnetic Bragg harmonics. To date these additional Bragg reflections have not been observed directly in an experiment. As far as the spin dynamics is concerned, only the near-zone-boundary spin-wave dispersion relations were studied. For the physics of the incommensurate state, it is the the low-energy, small-Q spin excitations that are most relevant. In the present work we continue our studies of $Ba_2CuGe_2O_7$, investigating the field dependence of higher-order magnetic Bragg peaks and the low-energy spin-wave spectrum in both the incommensurate and commensurate states. We find that even in the absence of an external magnetic field the spiral structure is distorted by the presence of previously disregarded magnetic anisotropy. Our results are consistent with the theoretical predictions of Kaplan[17] and Shekhtman, Entin-Wohlman, and Aharony,[18,19] who demonstrated that a generic anisotropy term must inevitably accompany Dzyaloshinskii-Moriya interactions. The understanding of the physics of $Ba_2CuGe_2O_7$ enables us to refine our interpretation of previously obtained experimental data. A brief report on some of our results is published elsewhere.[20]

II. EXPERIMENT

Neutron diffraction and inelastic neutron-scattering measurements were performed in two series of experiments, on the IN-14 3-axis spectrometer at the Institut Laue Langevein (ILL) in Grenoble, and the SPINS spectrometer at the Cold Neutron Research Facility at the National Institute of Standards and Technology (NIST). Single-crystal samples of $Ba_2CuGe_2O_7$ rarely survive more than one cooling to low temperatures. Two different crystals, prepared by the floating-zone method, were used in the two experimental runs. Sample A, a cylindrical single crystal of dimensions $4\times4\times20$ mm^3 was used in experiments at IN-14, but spontaneously disintegrated during subsequent storage. Sample B was used in the second experiment on SPINS and was approximately $6\times6\times50$ mm^3. The crystal mosaic was around 0.35° full width at half maximum (FWHM) for sample A and 1.2° FWHM for sample B, as measured in the (a,b) crystallographic plane. The mosaic spread in the perpendicular direction was measured for sample B and found to be around 2° FWHM. The samples were mounted on the spectrometers with their c axes vertical, making $(h,k,0)$ wave vectors accessible for measurements. In both experiments the magnetic field was produced by standard split-coil superconducting magnets. The alignment of the c axis of the crystal with the direction of the magnetic field, previously shown to be crucial for high-field measurements,[14] was around 1.4° in both runs, as measured at low temperatures. The measurements were performed in the field range 0–2.5 T. The sample environment was a pumped-^{4}He cryostat for the ILL experiment and a cryopump-driven ^{3}He cryostat at NIST. The data were collected at temperatures in the range 0.35–5 K. As observed previously, cooling the sample through T_N in an $H\approx1$ T magnetic field always resulted in a single-domain magnetic structure.

The spin-wave dispersion was measured in constant-Q scans in the range of energy transfers 0–0.8 meV. Neutrons of 3.5 or 2.5 meV fixed incident energy were used in most cases. Alternatively, a 3.5 meV fixed final-energy setup was exploited. A Be filter was positioned in front of the sample to eliminate higher-order beam contamination. $40'-S-40'-A-40'$ collimations were utilized in both runs. The typical energy resolution with 3.5 meV incident energy neutrons was 0.075 meV FWHM, as determined from measurements of incoherent scattering from the sample.

III. RESULTS

A. Higher-order Bragg reflections

In previous studies the only magnetic elastic peaks observed in $Ba_2CuGe_2O_7$ were those corresponding to an ideal

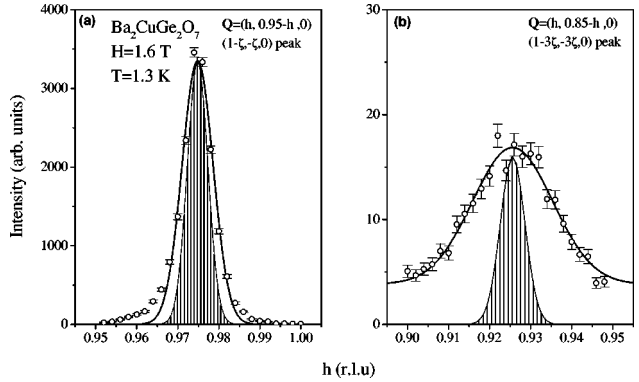

FIG. 2. Transverse elastic scans through the first-order (a) and third-order (b) magnetic Bragg reflections measured in $Ba_2CuGe_2O_7$ at $T=1.3$ K and $H=1.6$ T. Solid lines are Gaussian fits to the data. The shaded Gaussian represents the calculated experimental Q resolution. The intrinsic angular width of both peaks is $\approx 20°$ as seen from the (1,0,0) antiferromagnetic zone center.

sinusoidal spiral structure with propagation vectors $(1\pm\zeta, \pm\zeta,0)$. These reflections, whose intensity seems to account for almost 100% of the expected magnetic diffraction intensity appear below $T_N\approx 3.2$ K around antiferromagnetic zone centers $(h,k,0)$, h, k integer, $h+k$ odd. In the present study, careful elastic scans along the $(1+x,x,0)$ line in reciprocal space revealed the presence of additional extremely weak peaks at $(1\pm 3\zeta,\pm 3\zeta,0)$, as shown in Fig. 1. These peaks are clearly of magnetic origin, as the temperature dependence of their intensity is similar to that of the principal magnetic reflections at $(1\pm\zeta,\pm\zeta,0)$. The additional third-order peak was observed in all magnetic fields in the range 0–1.9 T, and always appears at $(1\pm 3\zeta,\pm 3\zeta,0)$, where ζ, defined by the position of the principal magnetic Bragg peak, is itself field dependent.[13,14] For $0<H<1.7$ T the measured field dependence of ζ is in total agreement with previous studies. For the purpose of convenience we shall define $\boldsymbol{Q}_{\pi,\pi}=(1,0,0)$ (antiferromagnetic zone center), and $\boldsymbol{q}_0=(\zeta,\zeta,0)$. In this notation the first- and third-order magnetic reflections correspond to momentum transfers $\boldsymbol{Q}_{\pi,\pi}\pm\boldsymbol{q}_0$ and $\boldsymbol{Q}_{\pi,\pi}\pm 3\boldsymbol{q}_0$, respectively.

As observed previously, at $H=H_1\approx 1.7$ T (at $T=0.35$ K) the system goes through a magnetic transition to a different phase that is characterized by the appearance of a new peak at the commensurate (1,0,0) reciprocal-space position. As discussed previously, this phase may or may not be a result of the slight misalignment of the magnetic field relative to the c axis of the crystal. In the present work we did not investigate this ''intermediate'' phase in detail, performing most measurements in the field ranges $0<H<H_1$ and $H>H_c\approx 2.2$ T, where H_c is the magnetic field at which the structure becomes commensurate.[13,14]

In scans along the (1,1,0) direction, shown in Fig. 1, the widths of both first- and third-order peaks are resolution limited. This is not the case for transverse scans along $(1,\bar{1},0)$, where the first, and especially the third harmonic are visibly broader than the experimental resolution (Fig. 2). The observed peak width pattern is consistent with both peaks having a zero longitudinal and a 20° transverse intrinsic width *as seen from the* $\boldsymbol{Q}_{\pi,\pi}$ *reciprocal-space point*. The transverse intrinsic Q width of the third harmonic is thus three times as large as that of the first harmonic. This result does not appear to depend on the applied magnetic field or the history of the sample. The large observed transverse width is likely to be related to the previously established fact that the spiral structures propagating in any direction in the (001) plane have almost identical energies. The (1,1,0) direction is only slightly energetically preferable.[15] Due to pinning or even thermal fluctuations, in a macroscopic sample an entire ensemble of spiral structures with propagation directions fanning out around (1,1,0) will therefore be realized, producing substantial transverse peak widths.

The field dependence of the integrated peak intensities was measured in both field-cooling and zero-field cooling experiments. Consistent results were obtained in both types of measurement, and no signs of hysteresis were observed. In the ILL experiment the propagation direction of the spiral, always along (1,1,0) at $H=0$, was found to deviate by as much as several degrees from this direction in higher fields. This effect is clearly due to a slight misalignment of the magnetic field relative to the c axis, and the possibility to almost freely rotate the magnetic propagation vector in the (a,b) crystallographic plane.[15] In the NIST experiment such a deviation was not observed, thanks to a slightly different and more ''fortunate'' setting of the sample. The field dependence of the peak intensities was therefore measured in this second experimental run, but, just in case, at each field, both the first- and third-order peaks were centered in a series of transverse and longitudinal scans. The measured integrated intensity of the first and third-order reflection, as well as that of the commensurate peak at (1,0,0), are plotted against magnetic field applied along the c axis in Fig. 3. The total intensity of all three features is field independent within experimental error.

As seen in Fig. 3, the intensity of the $(1+\zeta,\zeta,0)$ magnetic reflection is almost field independent in the range $0<H<H_1$. This appears to be in contradiction with previous measurements [Ref. 14, Fig. 3(d)], where a gradual decrease of the intensity of the first harmonic was observed with increasing magnetic field. However, we now know what was wrong with these previous measurements: the possibility of the propagation vector deviating from the (1,1,0) direction was not taken into account. In a slightly misaligned sample the field-induced drift of the magnetic reflections away from the line of the elastic scan was incorrectly interpreted as a decrease of peak intensity. Note that in the present study the centering of the peaks at each field ensures that this problem, even if present, does not influence the measurements.

B. Spin waves

All inelastic measurements were done in the vicinity of the (1,0,0) antiferromagnetic zone center ($\boldsymbol{Q}\approx\boldsymbol{Q}_{\pi,\pi}$). The spin-wave dispersion was measured along the $(1+\epsilon,\epsilon,0)$ direction (x axis). In most cases the sample was field cooled to eliminate the need to deal with inelastic signal coming from the two magnetic domains. All scans at $\boldsymbol{Q}=\boldsymbol{Q}_{\pi,\pi}$ were repeated using zero-field cooling to ensure that no hysteresis effects influence the measurements. The most important limiting factor in these inelastic studies is the presence of incoherent scattering and magnetic Bragg tails, centered at zero energy transfer. This undesirable contamination is absent for

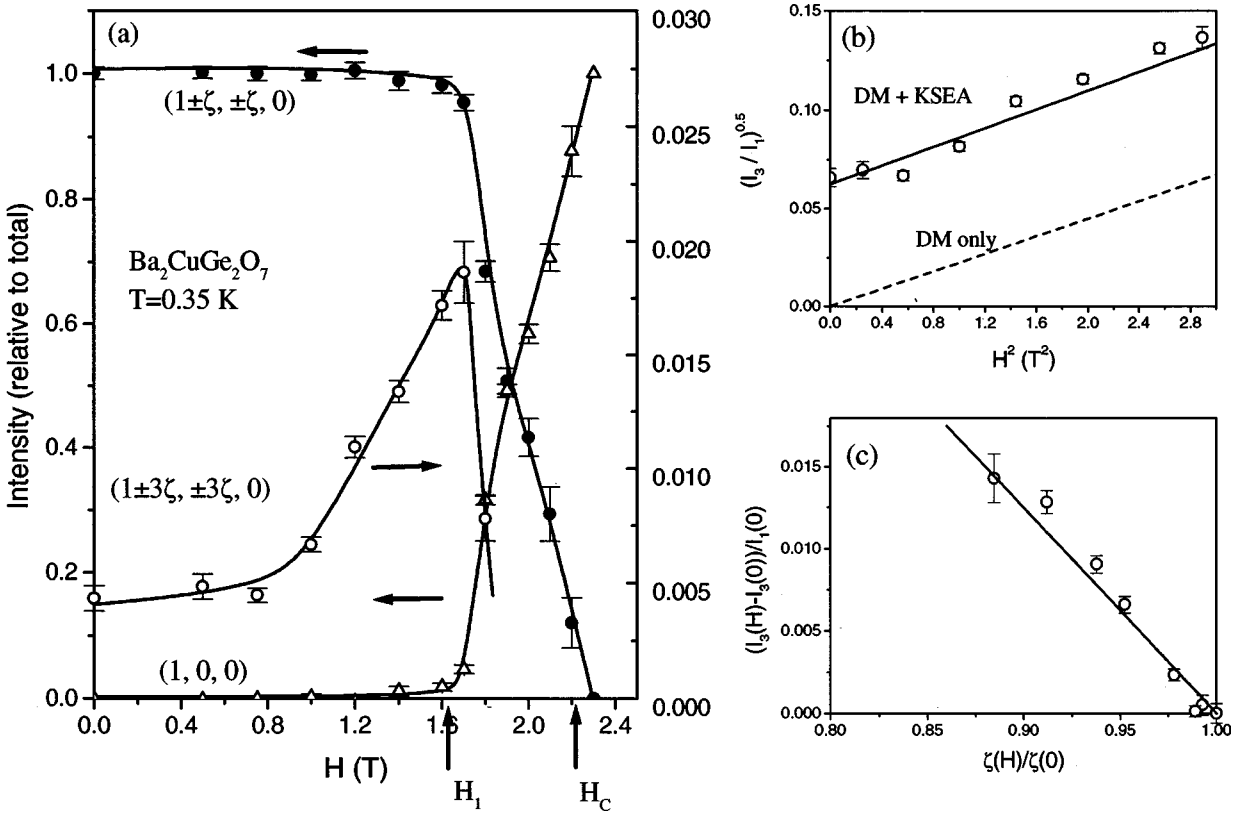

FIG. 3. (a) Measured field dependence of the magnetic Bragg peak intensities in $Ba_2CuGe_2O_7$ at $T=0.35$ K. Solid and open circles show the behavior of the first-order and third-order incommensurate Bragg peak integrated intensities, respectively. The intensity of the commensurate peak at the antiferromagnetic zone center is plotted in open triangles. (b) Square root of the ratio of intensities of the third and first harmonic plotted against the square of the applied magnetic field. The solid and dashed lines show the theoretical prediction for the DM-only and DM+KSEA models. (c) Measured intensity of the third harmonic plotted against the normalized incommensurability parameter ζ. The solid line shows the prediction of the DM+KSEA model.

energy transfers $(\hbar\omega)\gtrsim 0.15$ meV, where reliable data could be collected. Typical constant-Q scans obtained in the ILL and NIST experiments are shown in Fig. 4. Peak positions were determined by fitting Gaussian profiles to the data. All the inelastic peaks studied were found to be resolution limited. The focusing conditions are considerably more favorable at $\boldsymbol{Q}=(1+\epsilon,\epsilon,0)$, $\epsilon>0$, where most of the measurements were performed.

1. Zero field

The dispersion relation measured in zero applied field is plotted in symbols in Fig. 5. One clearly sees three distinct branches of the spectrum. These we shall label by the wave vectors to which they extrapolate at zero energy transfer: $\boldsymbol{Q}_{\pi,\pi}\pm\boldsymbol{q}_0$ and $\boldsymbol{Q}_{\pi,\pi}$, correspondingly. An obvious and very interesting feature is the ''repulsion'' between the $\boldsymbol{Q}_{\pi,\pi}\pm\boldsymbol{q}_0$ branches at their point of intersection $\boldsymbol{Q}=\boldsymbol{Q}_{\pi,\pi}$. Its magnitude is given by the splitting $2\delta_{\pi,\pi}\approx 0.12(1)$ meV. This effect again manifests itself at $\boldsymbol{Q}_{\pi,\pi}+2\boldsymbol{q}_0$, where it is seen as a discontinuity in the $\boldsymbol{Q}_{\pi,\pi}\pm\boldsymbol{q}_0$ branch. Simple empirical fits to the data (not shown) allow us to estimate the spin-wave velocity $c_0\approx 5.21(3)$ meV Å. This value is in reasonable agreement with the estimate $c_0=Ja/\sqrt{2}\approx 5.75$ meV Å, obtained using the classical formula (3) in Ref. 1 and the exchange constant $J\approx 0.96$ meV, previously determined from measuring the spin-wave bandwidth. The main characteristic of the $\boldsymbol{Q}_{\pi,\pi}$ branch is the energy gap $\Delta_{\pi,\pi}\approx 0.18(1)$ meV at the antiferromagnetic zone center $\boldsymbol{Q}_{\pi,\pi}$.

2. Field dependence in the incommensurate phase $(H<H_1)$

In Fig. 6 we show the spin-wave dispersion measured in $Ba_2CuGe_2O_7$ in a $H=1$ T magnetic field applied along the c axis of the crystal. In this case the incommensurability parameter $\zeta(H=1\ \text{T})=0.0252(5)$. The $\boldsymbol{Q}_{\pi,\pi}\pm\boldsymbol{q}_0$ dispersion curves are very similar to those measured in zero field and appear to be adequately described by the same spin-wave velocity and splitting parameter $2\delta_{\pi,\pi}$. Compared to the zero-field case however, at $H=1$ T the central $\boldsymbol{Q}_{\pi,\pi}$ branch is visibly flattened at its minimum. The gap $\Delta_{\pi,\pi}$ in this mode is equal to ≈ 0.24 meV. Comparing this to $\Delta_{\pi,\pi}=0.18$ meV at $H=0$, we find that, to a good approximation

$$\Delta_{\pi,\pi}(H)^2=\Delta_{\pi,\pi}^2+(2g_cS\mu_BH)^2, \tag{1}$$

where $g_c=2.474$ is the c-axis diagonal component of the gyromagnetic ratio for Cu^{2+} in $Ba_2CuGe_2O_7$ (Ref. 21), $S=1/2$ is the spin of Cu^{2+} ions and μ_B is the Bohr magneton. At $H=1$ T the measured dispersion curve for the $\boldsymbol{Q}_{\pi,\pi}$

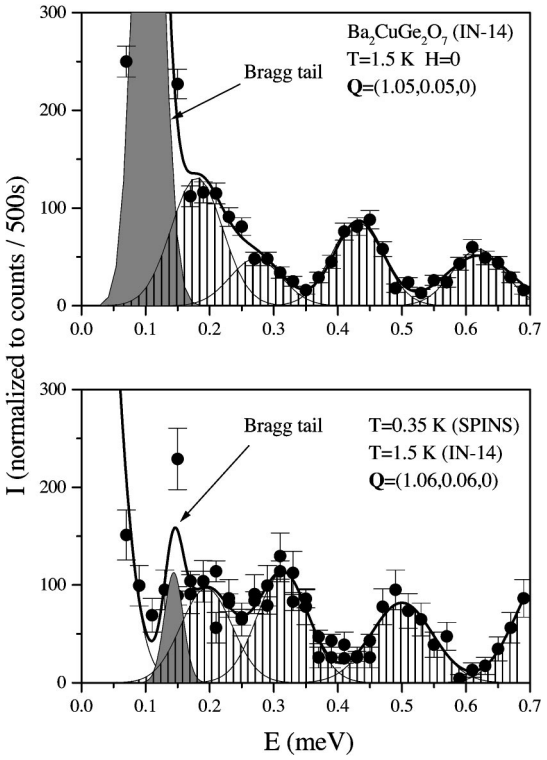

FIG. 4. Typical inelastic scans measured in $Ba_2CuGe_2O_7$ in the two experimental runs, at ILL (top) and NIST (bottom), respectively. The heavy solid line is a multiple-Gaussian fit to the data, and the shaded curves represent the individual Gaussians. The gray area in the top panel shows the position of a ''Bragg-tail'' spurious peak.

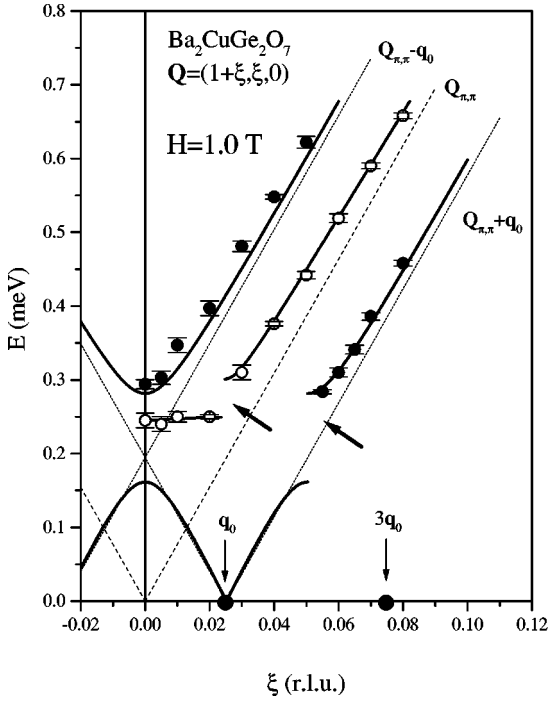

FIG. 6. Spin-wave dispersion curves measured in $Ba_2CuGe_2O_7$ in a $H=1$ T magnetic field applied along the (001) direction at $T=0.35$ K. Solid lines are guides for the eye. Dashed lines are as in Fig. 5.

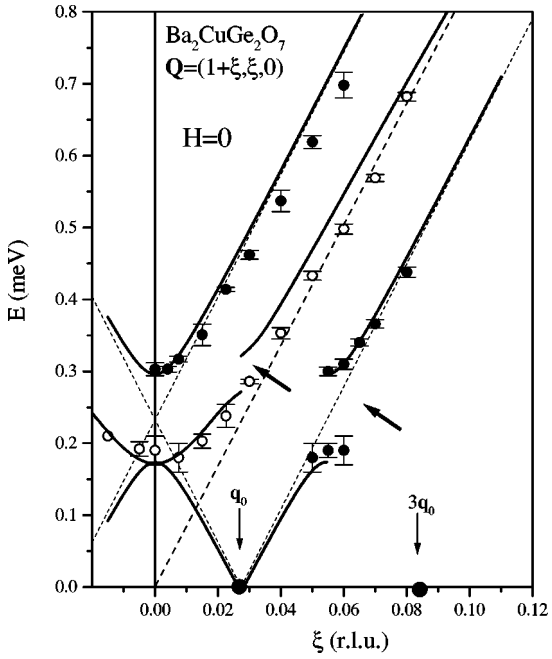

FIG. 5. Spin-wave dispersion curves measured in $Ba_2CuGe_2O_7$ in zero magnetic field. The data collected at $T=0.35$ K and $T=1.5$ K are combined in this plot. The solid lines are parameter-free theoretical curves as described in the text. Dashed lines are guides for the eye and the solid circles on the abscissa show the positions of the observed magnetic Bragg peaks.

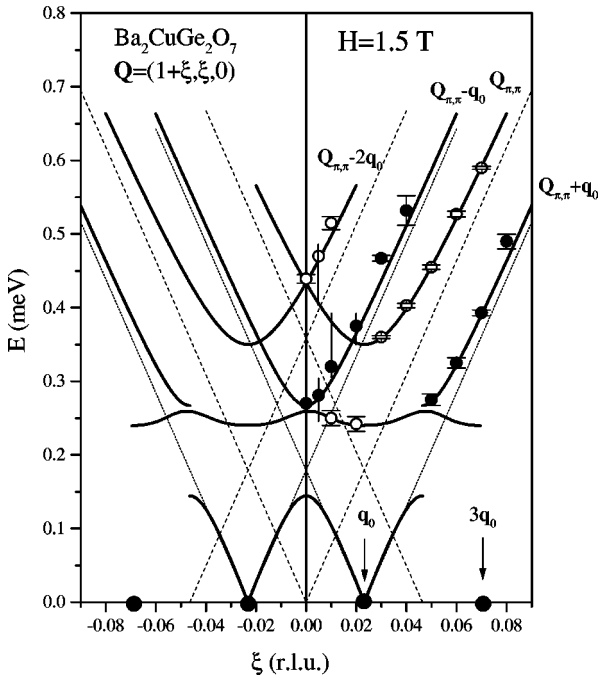

FIG. 7. Spin-wave dispersion curves measured in $Ba_2CuGe_2O_7$ in a $H=1.5$ T magnetic field applied along the (001) direction at $T=0.35$ K. The lines and symbols as in previous figures. Note the additional branch in the spectrum.

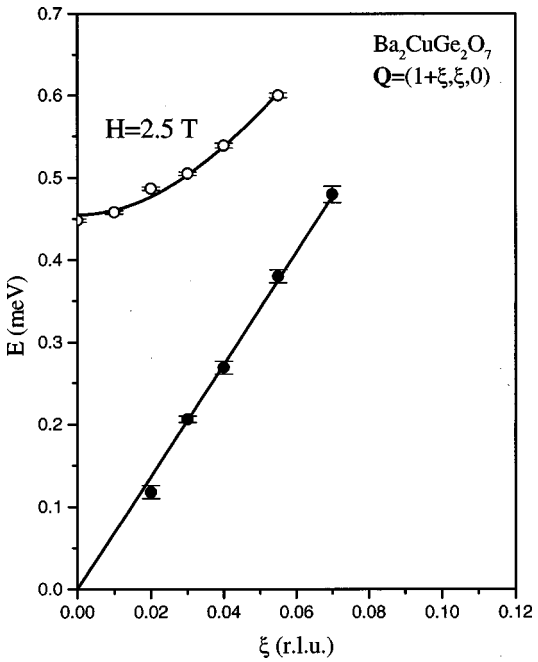

FIG. 8. Spin-wave dispersion curves measured in $Ba_2CuGe_2O_7$ in a $H=2.5$ T magnetic field applied along the (001) direction at $T=0.35$ K (commensurate spin-flop phase). The upper solid line is a fit to Eq. (2). The lower line is a linear fit.

branch has a different feature, namely a discontinuity at $\boldsymbol{Q}_{\pi,\pi}+\boldsymbol{q}_0$. This splitting, that we shall denote as $2\delta_{\boldsymbol{q}_0}$, is roughly 0.05 meV.

In a magnetic field $H=1.5$ T$\simeq H_{c1}$ ($\zeta=0.0232$) the spectrum becomes substantially more complex (Fig. 7). The two $\boldsymbol{Q}_{\pi,\pi}\pm\boldsymbol{q}_0$ modes remain essentially unchanged. The $\boldsymbol{Q}_{\pi,\pi}$ gap in the central branch is $\Delta_{\boldsymbol{Q}_{\pi,\pi}}(H)\approx 0.28$ meV, which is consistent with Eq. (1). The discontinuity at $\boldsymbol{Q}_{\pi,\pi}+\boldsymbol{q}_0$ is clearly visible in $H=1.5$ T data: $2\delta_{\boldsymbol{q}_0}\approx 0.11$ meV. Another feature of the spectrum that is not visible in lower applied fields is the presence of a different excitation branch that at $\boldsymbol{Q}_{\pi,\pi}$ is seen at $(\hbar\omega)\approx 0.45$ meV. The shortage of beam time prevented us from following this branch to lower energy transfers (where its intensity should increase) at wave vectors where it would appear focusing: all measurements were done at $\boldsymbol{Q}=(1+\epsilon,\epsilon,0)$, $\epsilon>0$. The limited data that we have at this stage is totally consistent with the new branch being a replica of the $\boldsymbol{Q}_{\pi,\pi}$ mode, but centered at $\boldsymbol{Q}_{\pi,\pi}\pm 2\boldsymbol{q}_0$, as shown by the corresponding solid lines in Fig. 7.

3. High field: commensurate phase

The dispersion relations measured at $H=2.5$ T, well above $H_c\approx 2.2$ T, are shown in Fig. 8. As expected for the commensurate state, only two branches are present. Two peculiarities are to be noted here. First, the measured spin-wave velocity $c_0=4.83(3)$ meV Å is significantly smaller than that seen at $H<H_c$. Second, the gap in the higher-energy branch (≈ 0.45 meV) is too large to be accounted for by the effect of magnetic field alone ($2g_cS\mu_BH=0.36$ meV). If for this branch we can write

$$(\hbar\omega)^2=\Delta_c^2+(2g_cS\mu_BH)^2+c_0^2q^2, \tag{2}$$

for the ''additional'' gap in the commensurate phase we obtain $\Delta_c=0.28(1)$ meV (solid lines in Fig. 8).

IV. THEORY

Most of the magnetic properties of $Ba_2CuGe_2O_7$ reported to date appeared to be rather well described by a simple spin Hamiltonian that included only nearest-neighbor Heisenberg antiferromagnetic exchange interactions and the Dzyaloshinskii-Moriya cross-product terms. For reasons that will shortly become apparent we shall refer to this construct as the ''DM-only'' model for $Ba_2CuGe_2O_7$. For a single Cu plane in $Ba_2CuGe_2O_7$ the Hamiltonian takes the form

$$\begin{aligned}\mathcal{H}&=\mathcal{H}^{(\mathrm{H})}+H^{(\mathrm{DM})}\\&=\sum_{n,m}\{J(\boldsymbol{S}_{n,m}\cdot\boldsymbol{S}_{n+1,m}+\boldsymbol{S}_{n,m}\cdot\boldsymbol{S}_{n,m+1})+D[(\boldsymbol{S}_{n,m}\\&\quad\times\boldsymbol{S}_{n+1,m})_y+(\boldsymbol{S}_{n,m}\times\boldsymbol{S}_{n,m+1})_x]\}.\end{aligned} \tag{3}$$

Here the indexes n and m enumerate the Cu^{2+} spins along the x and y axes, respectively, $\boldsymbol{S}_{n,m}$ are the site spin operators, J is Heisenberg exchange constant, and D is the norm of the Dzyaloshinskii vector. Microscopically, the Heisenberg term $\mathcal{H}^{(\mathrm{H})}$ represents the Anderson superexchange mechanism.[22] It arises from virtual *non-spin-flop* hopping of two electrons onto a nonoccupied orbital, where they interact via Pauli's exclusion principle. As shown by Moriya,[5] the cross-product term $\mathcal{H}^{(\mathrm{DM})}$ originates from *spin-flop* hopping, which is made possible by spin-orbit interactions.

The classical ground state of the DM-only model is an ideal sinusoidal spin spiral. The experimental observation of higher-order magnetic reflections in zero magnetic field tells us that this model is not a fully adequate description of $Ba_2CuGe_2O_7$: something is missing from the Hamiltonian (3). To understand what is going on we first note that for two spins $\boldsymbol{S}_1$ and $\boldsymbol{S}_2$, interacting via isotropic exchange and the Dzyaloshinskii-Moriya term, the interaction energy is minimized at $-\sqrt{J^2+D^2}S^2$ when both spins $\boldsymbol{S}_1$ and $\boldsymbol{S}_2$ are perpendicular to $\boldsymbol{D}$, forming the angle $\pi+\alpha$, where $\alpha=\arctan(D/J)$. Therefore, the Dzyaloshinskii-Moriya cross-product term $\mathcal{H}^{(\mathrm{DM})}$ lifts the local O(3) symmetry of the Heisenberg Hamiltonian and creates an effective easy-plane anisotropy of strength $\sqrt{J^2+D^2}-J\simeq D^2/2J$.

Relatively recently Kaplan[17] and Shekhtman, Entin-Wohlman, and Aharony[18] (KSEA) argued that in most realizations of Moriya's superexchange mechanism this apparent easy-plane anisotropy is an artifact of the omission of terms quadratic in D in the expansion of the true Hamiltonian of the system. If such terms are properly included, the O(3) symmetry of a single bond is restored by an additional term $(\sqrt{J^2+D^2}-J)/D^2\,(\boldsymbol{S}_1\cdot\boldsymbol{D})\,(\boldsymbol{S}_2\cdot\boldsymbol{D})\simeq(1/2J)\,(\boldsymbol{S}_1\cdot\boldsymbol{D})\,(\boldsymbol{S}_2\cdot\boldsymbol{D})$. Note that this additional interaction has the form of easy-axis two-ion anisotropy and its strength is such that it *exactly* compensates the easy-plane effect of the Dzyaloshinskii-Moriya cross product. With this term included, the ground state of the two-spin Hamiltonian has full O(3) symmetry. The energy of two interacting spins pointing parallel and antiparallel to $\boldsymbol{D}$, respectively, is exactly equal to that of two spins perpendicular to $\boldsymbol{D}$ and forming the angle $\pi+\alpha$ be-

tween themselves. We shall refer to this ''hidden symmetry'' term as the KSEA anisotropy term or KSEA interaction. For a recent discussion of this subject see Ref. 23.

To properly account for KSEA interactions in our model of $Ba_2CuGe_2O_7$, where $D \ll J$, the spin Hamiltonian can be rewritten as follows:

$$\begin{aligned}\mathcal{H} &= \mathcal{H}^{(\mathrm{H})} + H^{(\mathrm{DM})} + H^{(\mathrm{KSEA})} \\ &= \sum_{n,m} \Big[J(\boldsymbol{S}_{n,m}\cdot\boldsymbol{S}_{n+1,m} + \boldsymbol{S}_{n,m}\cdot\boldsymbol{S}_{n,m+1}) \\ &\quad + D[(\boldsymbol{S}_{n,m}\times\boldsymbol{S}_{n+1,m})_y + (\boldsymbol{S}_{n,m}\times\boldsymbol{S}_{n,m+1})_x] \\ &\quad + \frac{D^2}{2J}(S^y_{n,m}S^y_{n+1,m} + S^x_{n,m}S^x_{n,m+1}) \Big]. \end{aligned} \tag{4}$$

Can this Hamiltonian (the ''DM+KSEA'' model) account for both recent and previously published experimental data on $Ba_2CuGe_2O_7$? In the following sections we shall systematically investigate the effect of the KSEA term on static and dynamic properties of a DM helimagnet, and show that indeed it can.

A. Static properties

1. Free energy in the continuous limit

As the period of the spiral structure in $Ba_2CuGe_2O_7$ is rather long ($\approx$36 lattice spacings), we can safely use the continuous approximation to describe it.[14,15] In this framework the magnetic free energy is expanded as a functional of a slowly rotating unitary vector field $\boldsymbol{n}(\boldsymbol{r})$. At each point in space $\boldsymbol{n}(\boldsymbol{r})$ is chosen along the local staggered magnetization. The Hamiltonian (3) then gives rise to the following free energy functional:

$$\begin{aligned}F^{(\mathrm{DM})} = \int dx\,dy \Bigg\{ \frac{\rho_s}{2}\Bigg[\left(\partial_x\boldsymbol{n} - \frac{\alpha}{\Lambda}\boldsymbol{e}_y\times\boldsymbol{n}\right)^2 + \left(\partial_y\boldsymbol{n} - \frac{\alpha}{\Lambda}\boldsymbol{e}_x\times\boldsymbol{n}\right)^2 \Bigg] \\ - \frac{\alpha^2}{2\Lambda^2}\rho_s n_z^2 + \frac{(\chi_\perp - \chi_\parallel)(\boldsymbol{H}\cdot\boldsymbol{n})^2}{2} - \frac{\chi_\perp H^2}{2} \Bigg\}. \end{aligned} \tag{5}$$

In this formula ρ_s is the spin stiffness, that in the classical model at $T=0$ is given by $\rho_s = S^2\sqrt{J^2+D^2} \approx S^2 J$, α as before is the equilibrium angle between two spins defined as $\alpha = \arctan(D/J)$, Λ is the nearest-neighbor Cu-Cu distance, $\chi_\parallel$ and $\chi_\perp$ are the local longitudinal and transverse magnetic susceptibilities, respectively. Their classical $T=0$ values are $\chi_\perp = (g\mu_B)^2/(4J\Lambda^2)$ and $\chi_\parallel = 0$, correspondingly. In Eq. (5) we have included the Zeeman term that represents interaction of the system with an external magnetic field $\boldsymbol{H}$.

The term $-\alpha^2\rho_s n_z^2/2\Lambda^2$ in Eq. (5) deserves some comment. It has the form of a magnetic easy-z-axis anisotropy and represents the combined effect of the effective (xz) and (yz) easy planes produced by DM interactions on the y and x bonds, respectively. This term is *eliminated* by KSEA interactions that modify Eq. (5) as follows:

$$\begin{aligned}F^{(\mathrm{DM+KSEA})} = \int dx\,dy \Bigg\{ \frac{\rho_s}{2}\Bigg[\left(\partial_x\boldsymbol{n} - \frac{\alpha}{\Lambda}\boldsymbol{e}_y\times\boldsymbol{n}\right)^2 \\ + \left(\partial_y\boldsymbol{n} - \frac{\alpha}{\Lambda}\boldsymbol{e}_x\times\boldsymbol{n}\right)^2 \Bigg] \\ + \frac{(\chi_\perp - \chi_\parallel)(\boldsymbol{H}\cdot\boldsymbol{n})^2}{2} - \frac{\chi_\perp H^2}{2} \Bigg\}. \end{aligned} \tag{6}$$

This equation is in agreement with Eq. (3) in Ref. 15. Comparing Eqs. (3) and (6) one concludes that *in the continuous limit* for the square-lattice spin arrangement found in $Ba_2CuGe_2O_7$, KSEA interactions (two sets of easy axes, for x and y bonds, respectively) are indistinguishable from an overall easy-(xy)-plane anisotropy of relative strength $\delta = \alpha^2/2$.

In this work we are mostly concerned with the effect of a magnetic field applied along the [001] crystallographic direction, i.e., along the z axis. Under these conditions the propagation direction of the spin spiral in $Ba_2CuGe_2O_7$ is either along the x or y axis (two domain types are possible). Moreover, as we shall prove rigorously while discussing the spin waves in the system, the magnetic structure remains *planar* despite the two types of Dzyaloshinskii vectors, along the x and y axes (for the y and x bonds, respectively). This fact allows us to write the components of vector $\boldsymbol{n}(\boldsymbol{r})$ as $[\sin\theta(x), 0, \cos\theta(x)]$, where $\theta(x)$ is the angle between local staggered moment $\boldsymbol{n}(\boldsymbol{r})$ and the z axis, for a helix propagating along the x direction. The free energy can be then rewritten in terms of the $\theta(x)$ as

$$\begin{aligned}F^{(\mathrm{DM+KSEA})} = \int dx\,dy \Bigg[\frac{\rho_s[\partial_x\theta - (\alpha/\Lambda)]^2}{2} \\ + \left(\frac{\alpha^2\rho_s}{2\Lambda^2} + \frac{(\chi_\perp - \chi_\parallel)H^2}{2}\right)\cos^2\theta - \frac{\chi_\perp H^2}{2} \Bigg]. \end{aligned} \tag{7}$$

This is *exactly* Eq. (1) of Ref. 13 modified to include the effects of an easy (xy) plane anisotropy $\rho_s\alpha^2 n_z^2/2\Lambda^2 = \mathrm{const} - \rho_s\alpha^2\cos^2\theta/2\Lambda^2$, coming from the KSEA interaction on y bonds. As seen from this equation the sole effect of such anisotropy is to renormalize the external field to

$$H_{\mathrm{eff}}(H) = \sqrt{H^2 + \alpha^2\rho_s/\Lambda^2(\chi_\perp - \chi_\parallel)}. \tag{8}$$

2. Critical field and magnetic propagation vector

One important consequence of what is said above is that all our previous results, obtained in Refs. 13 and 14, can be *recycled* by substituting $H_{\mathrm{eff}}(H)$ for H in all formulas. Our conclusions regarding the field-induced commensurate-incommensurate Dzyaloshinskii transition in $Ba_2CuGe_2O_7$ remain valid in the presence of KSEA interaction. The KSEA interaction, however, modifies the value of the critical field H_c. Indeed, substituting $H_{\mathrm{eff}}(H)$ for H in Eq. (5) of Ref. 13 one gets $\sqrt{H_c^2 + \alpha^2/\Lambda^2\rho_s/(\chi_\perp - \chi_\parallel)} = (\pi\alpha/2\Lambda)\sqrt{\rho_s/(\chi_\perp - \chi_\parallel)}$. From this we immediately obtain

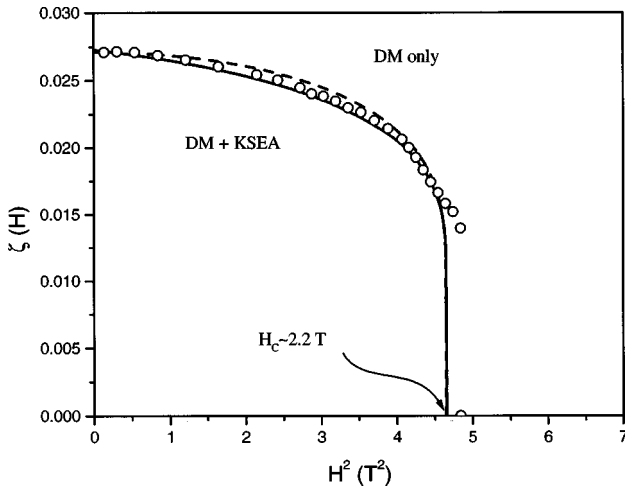

FIG. 9. Field dependence of the incommensurability parameter ζ, as previously measured in $Ba_2CuGe_2O_7$. The solid curve is plotted using Eqs. (10) and (11), that takes into account KSEA anisotropy. The dashed curve is the prediction of the DM-only model.

$$H_c = \alpha \frac{\sqrt{\pi^2-4}}{2\Lambda}\sqrt{\frac{\rho_s}{\chi_\perp - \chi_\parallel}}. \tag{9}$$

We see that the KSEA term reduces the critical field by the universal factor $\sqrt{1-4/\pi^2}\simeq 0.771$.

In order to obtain the field dependence of the inverse period of the structure ζ one has to rewrite Eqs. (4) and (7) of Ref. 13 as

$$\frac{2\pi\zeta(H)}{\alpha} = \frac{\pi^2}{4E(\beta)K(\beta)}, \tag{10}$$

$$\frac{H_{\rm eff}(H)}{H_{\rm eff}(H_c)} = \frac{\beta}{E(\beta)}. \tag{11}$$

Here β is an implicit variable. In case when the deformation of the spiral is weak $[(\alpha - 2\pi\zeta(H))/\alpha \ll 1]$, one can safely use the linearized formula:

$$\frac{2\pi\zeta(H)}{\alpha} = 1 - \frac{1}{32}\left(\frac{\pi H_{\rm eff}(H)}{2H_{\rm eff}(H_c)}\right)^4 + \text{higher-order terms}. \tag{12}$$

From this formula one can derive by how much KSEA interactions deform the spiral in zero external field. Let us define $\phi = 2\pi\zeta(0)$ as the average angle between spins in the spiral in zero field. This parameter is easily accessible experimentally and equal to $\phi = 2\pi \times 0.0273 = 0.172 \simeq 10°$.

Recalling that $H_{\rm eff}(0)/H_{\rm eff}(H_c) = 2/\pi$ and plugging it in Eq. (12) one gets $\phi/\alpha \simeq 1 - 1/32$ or

$$\alpha \equiv \arctan(D/J) = \frac{32}{31}\phi = \frac{32}{31}2\pi\zeta(0). \tag{13}$$

The KSEA term thus increases the period of the structure in zero field by roughly 3%.

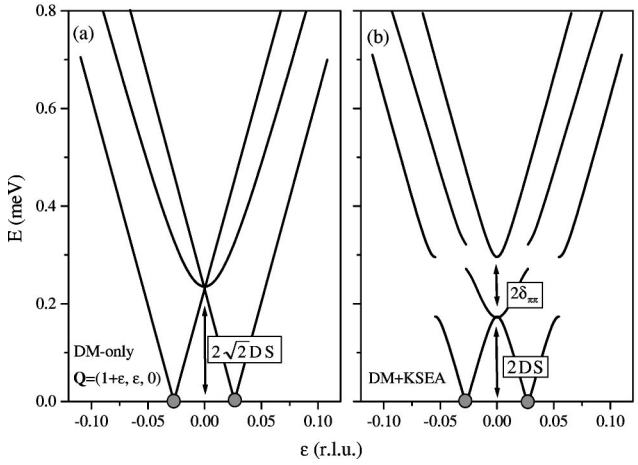

FIG. 10. Theoretical predictions for the spin-wave dispersion along the x axis in (a) the DM-only model, (b) DM+KSEA model. The effect of the KSEA term is to couple magnons separated by $2q_0$, which leads to the appearance of new gaps in the spectrum, and reduce the gap in $Q_{\pi,\pi}$ branch.

3. Higher-order Bragg harmonics

An important implication of Eq. (8) is that even in *zero* applied field the *effective* field is nonzero. The result is that the spiral structure is distorted even in zero field and higher-order (odd) magnetic Bragg peaks are present. To obtain a theoretical form for the field dependence of the third harmonic we can use Eqs. (17) and (18) in Ref. 14. More practical than the resulting expression is its linearized form, that applies in the limit $[\alpha - 2\pi\zeta(H)] \ll \alpha$ (weakly distorted spiral):

$$\frac{I_3}{I_1} = \frac{1}{256}\left(\frac{\pi H_{\rm eff}(H)}{2H_{\rm eff}(H_c)}\right)^4 = \frac{1}{256}\left[1 + \left(\frac{\pi^2}{4} - 1\right)\left(\frac{H}{H_c}\right)^2\right]^2. \tag{14}$$

Here I_1 and I_3 are the intensities of the first and third harmonic, respectively. One can see that for $H=0$ the third harmonic is predicted to be smaller than the first one by a factor of $1/256 \simeq 3.9\times 10^{-3}$.

Comparing Eqs. (14) and (12) one can see that for weak distortions the intensity of the third harmonic is proportional to the relative decrease of $\zeta(H)$:

$$\frac{\zeta(H)}{\zeta(0)} = 1 - \frac{8[I_3(H) - I_3(0)]}{I_1}. \tag{15}$$

4. Comparison with experiment

We now have to make sure that our results for the DM+KSEA model are consistent with both the previously published (Refs. 13 and 14) and new neutron-diffraction results on $Ba_2CuGe_2O_7$. First, let us compare the previously measured $\zeta(H)$ curve with the predictions of Eqs. (10) and (11). The experimental data for the incommensurability parameter (Ref. 13) is plotted against H^2 in Fig. 9. The solid line is the prediction of Eqs. (10) and (11). The dashed line is the theoretical curve previously obtained without including the KSEA term in the Hamiltonian.[13,14] In plotting both these

curves we have assumed the actual (measured) values for $H_c = 2.15$ T and $\zeta(0) = 0.0273$. Within experimental statistics it is practically impossible to distinguish between the two theoretical dependences and the data fits both of them reasonably well.

While it appears that the *shape* of the $\zeta(H)$ curve cannot be used to extract information on KSEA interactions, the actual numerical value of H_c in the DM-only and DM +KSEA models is substantially different. For the low-temperature limit in $Ba_2CuGe_2O_7$ we can use the classical expressions $\rho_s = JS^2 = 0.24$ meV, $\chi_\parallel = 0$, and $\chi_\perp = (g_c\mu_B)^2/8J\Lambda$, where $g_c = 2.47$ is the *c*-axis gyromagnetic ratio for Cu^{2+} in $Ba_2CuGe_2O_7$.[21] One can expect these classical estimates to be rather accurate, as they rely on the *effective* exchange constant J, that itself was determined from fitting the *classical* spin-wave dispersion relations to inelastic neutron-scattering data.[1] Substituting these values into Eq. (9) we immediately obtain $H_c^{(\mathrm{DM+KSEA})} = 2$ T. This is much closer to the experimental value $H_c = 2.15$ T, than the estimate $H_c^{(\mathrm{DM})} = 2.6$ T for the DM-only model.

The data for the field dependence of relative intensities of the first and third Bragg harmonics become consistent with theory only if KSEA interactions are properly taken into account. Indeed, the KSEA term is necessary to reproduce the observed distortion of the spiral in zero magnetic field. In Fig. 3(b) the solid lines are plotted using Eq. (14) and $H_c = 2.15$ T. The dashed lines are results for the intensity of the third Bragg harmonic obtained previously for the DM-only model.[14] Clearly the DM+KSEA model gives an excellent agreement with experiment [open symbols in Fig. 3(b)], while the DM-only Hamiltonian fails entirely to account for the available data.

In Fig. 3(c) we check the validity of theoretical prediction of Eq. (15), which is supposed to hold both with and without KSEA terms. The excellent agreement of theory and experiment confirms the validity of our picture of weakly deformed almost sinusoidal spiral.

B. Spin dynamics

We now turn to calculating the classical spin-wave spectrum in the DM+KSEA model for $Ba_2CuGe_2O_7$. This task will be accomplished in several separate steps. First, we shall derive the spectrum for a square-lattice Heisenberg Hamiltonian, including DM interactions only for the *x*-axis bonds. Second, we shall consider the effect of DM interactions along the *y*-axis bonds, showing that they do not disturb the planar spiral structure and do not influence the dispersion relation along the *x* direction. Next we shall analyze the effect of adding the KSEA term, following the method described in Refs. 24 and 25. While at this stage we do not have results for spin-wave dispersion in the DM+KSEA model in the presence of an arbitrary external magnetic field, we shall consider the case $H > H_c$ and derive an expression for Δ_c— the anisotropy gap in the commensurate state.

1. Dzyaloshinskii-Moriya interactions for x-axis bonds only

We start from a truncated version of the Hamiltonian (4):

$$\mathcal{H}^{(1)} = \sum_{n,m} [J\boldsymbol{S}_{n,m}\cdot\boldsymbol{S}_{n+1,m} + J\boldsymbol{S}_{n,m}\cdot\boldsymbol{S}_{n,m+1} + D(\boldsymbol{S}_{n,m}\times\boldsymbol{S}_{n+1,m})_y]. \tag{16}$$

It is easy to see that classically this Hamiltonian is minimized by a perfect helicoid propagating along the *x* axis with all spins lying in the (xz) plane:

$$\langle S^z_{n,m}\rangle = (-1)^{n+m}\langle S\rangle\cos n\alpha;$$
$$\langle S^x_{n,m}\rangle = (-1)^{n+m}\langle S\rangle\sin n\alpha. \tag{17}$$

The standard procedure to calculate the spin-wave spectrum is to rewrite this Hamiltonian in terms of spin projections on the rotating coordinate system, where the direction of the equilibrium value of the spin at (n,m) defines the *local* z' axis in such a way that $\langle S^{z'}_{n,m}\rangle = (-1)^{n+m}\langle S\rangle$. We leave the y coordinate unchanged, and select the x' axis to be orthogonal to both z' and $y' = y$. Substituting $S^z_{n,m} = S^{z'}_{n,m}\cos n\alpha - S^{x'}_{n,m}\sin n\alpha$, $S^x_{n,m} = S^{x'}_{n,m}\cos n\alpha + S^{z'}_{n,m}\sin n\alpha$, and $S^y_{n,m} = S^{y'}_{n,m}$ in the Hamiltonian (16) and using $\alpha = \arctan(D/J)$ we obtain

$$\mathcal{H}^{(1)} = \sum_{n,m} [\sqrt{J^2+D^2}(S^{z'}_{n,m}S^{z'}_{n+1,m} + S^{x'}_{n,m}S^{x'}_{n+1,m}) + JS^{y'}_{n,m}S^{y'}_{n+1,m} + J\boldsymbol{S}'_{n,m}\cdot\boldsymbol{S}'_{n,m+1}]. \tag{18}$$

In these coordinates the Hamiltonian is simply that of a square lattice antiferromagnetic (AFM) with easy-plane exchange anisotropy on bonds along the *x* direction. In agreement with the discussion in Sec. IV A 1 the relative strength of this anisotropy is given by

$$\delta = \frac{\sqrt{J^2+D^2}-J}{J} \simeq \frac{D^2}{2J^2} \simeq \frac{\alpha^2}{2}. \tag{19}$$

Applying the Holstein-Primakoff formalism we write the spin projection operators as $S^{z'}_{n,m} = (-1)^{n+m}(S - a^\dagger_{n,m}a_{n,m})$, $S^{x'} = (-1)^{n+m}\sqrt{S/2}(a_{n,m} + a^\dagger_{n,m})$, $S^{y'} = i\sqrt{S/2}(a^\dagger_{n,m} - a_{n,m})$. From Eq. (16) it is then straightforward to extract the quadratic part of the spin-wave Hamiltonian:

$$\mathcal{H}^{(1)} = JS\sum_{n,m} (4a^\dagger_{n,m}a_{n,m} - a_{n,m}a_{n+1,m} - a_{n,m}a_{n,m+1} - a^\dagger_{n,m}a^\dagger_{n+1,m} - a^\dagger_{n,m}a^\dagger_{n,m+1}) - \delta(a^\dagger_{n,m} + a_{n,m}) \times (a^\dagger_{n+1,m} + a_{n+1,m})/2 + 2\delta a^\dagger_{n,m}a_{n,m}. \tag{20}$$

After performing Fourier and Bogolyubov transformations to diagonalize this Hamiltonian, one readily obtains the spin-wave spectrum:

$$\mathcal{E}(k_x,k_y) = JS\sqrt{[4+2\delta-\delta\cos k_x]^2 - [(2+\delta)\cos k_x + 2\cos k_y]^2}. \tag{21}$$

This spectrum has one Goldstone branch at $k_x = k_y = 0$, that corresponds to the continuous symmetry of a simultaneous

rotation of all spins in the (xz) plane. At $k_x=k_y=\pi$ the spectrum has a finite gap $4JS\sqrt{\delta}=2\sqrt{2}DS$ due to the easy (xz) plane anisotropy coming from the DM without KSEA correction.

Now we have to recall that in the above derivation the wave vectors k_x,k_y correspond to a *rotating* system of coordinates. They are thus distinct from the actual component of the scattering vector in a neutron experiment. To get the proper spin-wave spectrum one has to perform a reverse coordinate transformation to the laboratory system:

$$\begin{aligned}
S^z_{n,m}&=S^{z'}_{n,m}\cos n\alpha-S^{x'}_{n,m}\sin n\alpha\\
&=(-1)^{n+m}[(S-a^\dagger_{n,m}a_{n,m})\cos n\alpha\\
&\quad-\sqrt{S/2}(a_{n,m}+a^\dagger_{n,m})\sin n\alpha];\\
S^x_{n,m}&=S^{x'}_{n,m}\cos n\alpha+S^{z'}_{n,m}\sin n\alpha\\
&=(-1)^{n+m}[(S-a^\dagger_{n,m}a_{n,m})\sin n\alpha\\
&\quad+\sqrt{S/2}(a_{n,m}+a^\dagger_{n,m})\cos n\alpha];\\
S^y_{n,m}&=S^{y'}_{n,m}=i\sqrt{S/2}(a^\dagger_{n,m}-a_{n,m}).
\end{aligned}\tag{22}$$

The x-axis dispersion of three spin-wave branches in laboratory system is shown in Fig. 10(a). The dynamic structure factor $S^{yy}(\boldsymbol{Q},\omega)$ has a single magnon peak at the energy given by $\mathcal{E}(Q_x,Q_y)$ (the $\boldsymbol{Q}_{\pi,\pi}$ branch). The structure factors $S^{xx}(\boldsymbol{Q},\omega)$ and $S^{zz}(\boldsymbol{Q},\omega)$ each contain two magnon branches with dispersion relations given by $\mathcal{E}(Q_x+\pi+\alpha,Q_y+\pi)$, and $\mathcal{E}(Q_x+\pi-\alpha,Q_y+\pi)$ (the $\boldsymbol{Q}_{\pi,\pi}\pm\boldsymbol{q}_0$ branches). As expected, the zeroes of energy in these two modes are precisely at the positions of magnetic Bragg peaks at $\boldsymbol{Q}_{\pi,\pi}\pm\boldsymbol{q}_0$. A curious feature of this plot is that all three branches are nearly degenerate at the AFM zone center.

2. Dzyaloshinskii-Moriya interactions along y-axis bonds

Let us now consider Dzyaloshinskii-Moriya interactions for the bonds in the y direction. Their contribution to the spin Hamiltonian can be written as

$$\begin{aligned}
\mathcal{H}^{(2)}&=\sum_{n,m}D(S^y_{n,m}S^z_{n,m+1}-S^z_{n,m}S^y_{n,m+1})\\
&=\sum_{n,m}DS^y_{n,m}(S^z_{n,m+1}-S^z_{n,m-1})\\
&=iDS\sum_{n,m}(-1)^{n+m}\sin n\alpha[a_{n,m}a_{n,m+1}-a^\dagger_{n,m}a^\dagger_{n,m+1}]\\
&\quad+\text{third-order terms}.
\end{aligned}\tag{23}$$

The absence of terms of the first order in $a_{n,m}$ and $a^\dagger_{n,m}$ means that in the original (flat-spiral) spin configuration the force acting on each spin produced by the added Dzyaloshinskii-Moriya coupling on the y bonds is equal to zero. Thus, switching on the y-axis DM interactions *does not disturb* the planar helimagnetic ground state of the Hamiltonian $\mathcal{H}^{(1)}$, which therefore is also the ground state of $\mathcal{H}^{(2)}\equiv\mathcal{H}^{(\mathrm{H})}+\mathcal{H}^{(\mathrm{DM})}$. This *a posteriori* verifies our assumption that spins continue to lie in the x-z plane in the presence of Dzyaloshinskii-Moriya interactions on y bonds, made in Sec. IV A 1.

New terms *quadratic* in $a_{n,m}$ and $a^\dagger_{n,m}$ are indeed introduced by the Dzyaloshinskii-Moriya interactions on y bonds, and the spin-wave spectrum is thus altered. After Fourier transformation Eq. (23) becomes

$$\begin{aligned}
\mathcal{H}^{(2)}=\frac{iDS}{2}\sum_{k_x,k_y}\sin k_y[&a^\dagger(k_x,k_y)a^\dagger(-k_x+\pi+\alpha,-k_y+\pi)\\
&-a^\dagger(k_x,k_y)a^\dagger(-k_x+\pi-\alpha,-k_y+\pi)\\
&+a(k_x,k_y)a(-k_x+\pi-\alpha,-k_y+\pi)\\
&-a(k_x,k_y)a(-k_x+\pi+\alpha,-k_y+\pi)].
\end{aligned}\tag{24}$$

The analysis of this term for general k_y is rather complicated and should be done by matrix diagonalization similar to that described in the next subsection for calculating the effects of KSEA interactions. Fortunately, for spin waves propagating along the x axis ($k_x=0$ or $k_x=\pi$) the contribution of $\mathcal{H}^{(2)}$ is exactly zero, thanks to the $\sin k_y$ prefactor in Eq. (24). In other words, as long as we are concerned with spin waves propagating along the (110) direction in $Ba_2CuGe_2O_7$ we can totally disregard the contribution of Dzyaloshinskii-Moriya interactions along the y-axis bonds.

3. Influence of KSEA interactions

Having understood the spectrum for the DM-only model, we can proceed to include KSEA terms in our calculations. We first note that if our system were *one-dimensional*, the inclusion of the KSEA term would fully restore O(3) symmetry, making the commensurate and spiral phases degenerate. In terms of spin waves this would signify a complete softening of the $\boldsymbol{Q}_\pi$ magnon branch at the AF zone center $\boldsymbol{Q}_\pi$. As will be demonstrated below, in the case of a two-dimensional spin arrangement in $Ba_2CuGe_2O_7$ the magnon softening at $\boldsymbol{Q}_{\pi,\pi}$ produced by KSEA interactions is incomplete.

As discussed in Sec. IV A 3, in the presence of the KSEA term the ground state is a *distorted* flat spin spiral. In this situation the transition to a uniformly rotating coordinate system used in Sec. IV B 1 loses its usefulness. Instead, we must rotate the coordinate system for spin quantization at each site in such a way, that the z axis follows the rotation of the spins in the distorted helix:

$$\begin{aligned}
S^z_{n,m}&=(-1)^{n+m}[(S-a^\dagger_{n,m}a_{n,m})\cos\theta_{n,m}\\
&\quad-\sqrt{S/2}(a_{n,m}+a^\dagger_{n,m})\sin\theta_{n,m}];\\
S^x_{n,m}&=(-1)^{n+m}[(S-a^\dagger_{n,m}a_{n,m})\sin\theta_{n,m}\\
&\quad+\sqrt{S/2}(a_{n,m}+a^\dagger_{n,m})\cos\theta_{n,m}];\\
S^y_{n,m}&=S^{y'}_{n,m}=i\sqrt{S/2}(a^\dagger_{n,m}-a_{n,m}).
\end{aligned}\tag{25}$$

Here $\theta_{n,m}$ denotes the angle between the local spin axis and z axis in the x-z plane. The Hamiltonian $\mathcal{H}^{(1)}+\mathcal{H}^{(3)}$ (as explained above, $\mathcal{H}^{(2)}$ is not relevant to the dispersion along the x axis that we are interested in) is then rewritten as

$$\mathcal{H}^{(1)}+\mathcal{H}^{(3)}=J\sum_{n,m}\Bigg[-\frac{\cos(\theta_{n+1,m}-\theta_{n,m}-\alpha)}{\cos\alpha}\Bigg((S-a^{\dagger}_{n,m}a_{n,m})(S-a^{\dagger}_{n+1,m}a_{n+1,m})+\frac{S}{2}(a^{\dagger}_{n,m}+a_{n,m})(a^{\dagger}_{n+1,m}+a_{n+1,m})\Bigg)$$
$$-\frac{S}{2}(a^{\dagger}_{n,m}-a_{n,m})(a^{\dagger}_{n+1,m}-a_{n+1,m})-\cos(\theta_{n,m+1}-\theta_{n,m})\Bigg((S-a^{\dagger}_{n,m}a_{n,m})(S-a^{\dagger}_{n,m+1}a_{n,m+1})$$
$$+\frac{S}{2}(a^{\dagger}_{n,m}+a_{n,m})(a^{\dagger}_{n,m+1}+a_{n,m+1})\Bigg)-\frac{S}{2}(a^{\dagger}_{n,m}-a_{n,m})(a^{\dagger}_{n,m+1}-a_{n,m+1})$$
$$-\frac{\alpha^2}{2}\Bigg(\frac{S}{2}(a^{\dagger}_{n,m}-a_{n,m})(a^{\dagger}_{n+1,m}-a_{n+1,m})+\frac{S}{2}(a^{\dagger}_{n,m}+a_{n,m})(a^{\dagger}_{n,m+1}+a_{n,m+1})\sin\theta_{n,m}\sin\theta_{n,m+1}$$
$$+(S-a^{\dagger}_{n,m}a_{n,m})(S-a^{\dagger}_{n,m+1}a_{n,m+1})\cos\theta_{n,m}\cos\theta_{n,m+1}\Bigg)\Bigg]+\text{linear terms}. \tag{26}$$

If all angles $\theta_{n,m}$ in the above expression are given by the solution of the sin-Gordon equation determining the ground state, the linear terms will vanish: they represent a static uncompensated force acting on the spins and must not be present in an equilibrium spin configuration. In general, Eq. (26) cannot be diagonalized analytically. Fortunately, we are dealing with a rather weakly distorted structure and can safely restrict ourselves to calculating the effect of the KSEA term to the first order in δ. It is easy to show that the easy x-y plane anisotropy of strength δ deforms the spiral in such a way that is $\theta_{n,m}=qn+(\delta/4\alpha^2)\sin 2qn+O(\delta^2)$, where $q=\alpha-O(\delta^2)$. Therefore, within our accuracy one can assume $\theta_{n,m}\simeq\alpha n$ in Eq. (26). In particular the anisotropy dependence of $\cos(\theta_{n+1,m}-\theta_{n,m}-\alpha)\simeq\cos[q-\alpha+(\delta/4J\alpha^2)\sin 2qn+O(\delta^2)]\simeq 1+O(\delta^2)$ can be disregarded. With these simplifications and after Fourier transformation Eq. (26) becomes

$$\mathcal{H}^{(1)}+\mathcal{H}^{(3)}=J\sum_{k_x,k_y}\Bigg[\Bigg(4+\delta-\frac{\delta}{2}\cos k_y\Bigg)a(k_x,k_y)^{\dagger}a(k_x,k_y)-\Bigg(2\cos k_x+2\cos k_y+\frac{\delta}{2}\cos k_y\Bigg)$$
$$\times\frac{a(-k_x,-k_y)a(k_x,k_y)+a(-k_x,-k_y)^{\dagger}a(k_x,k_y)^{\dagger}}{2}+\Bigg(\frac{\delta}{2}+\frac{\delta}{4}\cos k_y\Bigg)[a(k_x+2\alpha,k_y)^{\dagger}a(k_x,k_y)$$
$$+a(k_x-2\alpha,k_y)^{\dagger}a(k_x,k_y)]+\frac{\delta}{4}\cos k_y\Bigg(\frac{a(-k_x+2\alpha,k_y)a(k_x,k_y)+a(-k_x+2\alpha,k_y)^{\dagger}a(k_x,k_y)^{\dagger}}{2}$$
$$+\frac{a(-k_x-2\alpha,k_y)a(k_x,k_y)+a(-k_x-2\alpha,k_y)^{\dagger}a(k_x,k_y)^{\dagger}}{2}\Bigg)\Bigg]. \tag{27}$$

From this equation we can already qualitatively understand the role of KSEA interactions. Their main impact is the introduction of terms that couple magnons with wave vectors that differ by $2\boldsymbol{q}_0$. This coupling will have the largest effect when acting on a pair of magnons of equal energies. The result will be discontinuities in the magnon branches at certain wave vectors, that for the distorted helix become new zone boundaries. This picture is very similar to the formation of a zone structure and zone-boundary energy gaps in a free-electron gas, subject to a weak periodic external potential. Another consequence of KSEA interaction is the reduction of the energy gap in the $\boldsymbol{Q}_{\pi,\pi}$ branch at $k_x=k_y=\pi$ from $2\sqrt{2}DS$ to $2DS$. However, contrary to the one-dimensional case this gap does not become zero, i.e., another Goldstone excitation does not appear in two dimensions. This can be derived by looking at the part of Eq. (27), which does not involve mixing of branches separated by $2\boldsymbol{q}_0$, and, therefore, yields to the standard analytical calculation.

To actually calculate the spin-wave spectrum we have to find a transformation of Bose operators that would diagonalize the Hamiltonian (27). This transformation must respect Bose commutation relations, and for a rather general case of helimagnetic structures is described in detail in Ref. 25. It is essentially a Bogolyubov transformation involving a column vector of four operators: $\hat{a}(k_x,k_y)=[a(k_x-\alpha,k_y)^{\dagger},a(-k_x+\alpha,-k_y),a(k_x+\alpha,k_y)^{\dagger},a(-k_x-\alpha,-k_y)]$. The relevant part of the Hamiltonian (27) can be written as $\mathcal{H}=(1/2)\Sigma_{kx,ky}\hat{a}(k_x,k_y)^{\dagger}\hat{V}\hat{a}(k_x,k_y)$, where the 4×4 matrix $\hat{V}$ is given by

$$\hat{V}=\begin{pmatrix} A(k_x-\alpha,k_y) & B(k_x-\alpha,k_y) & C(k_x-\alpha,k_y) & D(k_x-\alpha,k_y)\\ B(k_x-\alpha,k_y) & A(-k_x+\alpha,-k_y) & D(k_x-\alpha,k_y) & C(-k_x+\alpha,-k_y)\\ C(k_x+\alpha,k_y) & D(k_x+\alpha,k_y) & A(k_x+\alpha,k_y) & B(k_x+\alpha,k_y)\\ D(k_x+\alpha,k_y) & C(-k_x-\alpha,-k_y) & B(k_x+\alpha,k_y) & A(-k_x-\alpha,-k_y)\end{pmatrix}. \tag{28}$$

Here $A(k_x,k_y)=JS[2+3\delta-(\delta/2)\cos k_y]$, $B(k_x,k_y)=-JS[(2+2\delta)\cos k_x+2\cos k_y+\delta/2\cos k_y]$, $C(k_x,k_y)=JS[\delta/2+(\delta/4)\cos k_y]$, and $D(k_x,k_y)=JS(\delta/4)\cos k_y$. To diagonalize the spin-wave Hamiltonian and at the same time ensure the conservation of commutation relations we have to find a matrix $\hat{Q}$ such that $\hat{Q}^{\dagger}\hat{V}\hat{Q}$ is diagonal, while $\hat{Q}^{\dagger}\hat{g}\hat{Q}=\hat{g}$, where $\hat{g}$ is the diagonal matrix with diagonal elements $(1,-1,1,-1)$. This is equivalent to diagonalizing the matrix $\hat{g}\hat{V}$.[25]

To obtain numerical results that could be directly compared to our measurements on $Ba_2CuGe_2O_7$ we used the independently measured values for $J=0.96$ meV and $D/J\approx\arctan(D/J)\equiv\alpha=\frac{32}{31}\phi=0.177$. A numerical diagonalization of $\hat{g}\hat{V}(0,0)$ was performed using a MATHEMATICA software package to yield the eigenvalues $\mathcal{E}_0=0.172$ meV, $\mathcal{E}_1=0.297$ meV, and $\mathcal{E}_2=0.171$ meV. These are the energies of the $\boldsymbol{Q}_{\pi,\pi}(\mathcal{E}_0)$, and $\boldsymbol{Q}_{\pi,\pi}\pm\boldsymbol{q}_0(\mathcal{E}_1,\mathcal{E}_2)$ branches at the AFM zone center $\boldsymbol{Q}_{\pi,\pi}$. The splitting was predicted to be $2\delta_{\pi,\pi}=(\mathcal{E}_1-\mathcal{E}_2)=0.12$ meV. This value is indistinguishable from the actual splitting observed in $Ba_2CuGe_2O_7$, quoted in the previous section. We can also calculate the splitting in the $\boldsymbol{Q}_{\pi,\pi}$ branch at $\boldsymbol{Q}_{\pi,\pi}\pm\boldsymbol{q}$: $2\delta_{\boldsymbol{q}_0}=0.049$ meV. Experimentally, this splitting was not observed in zero field, but is small enough to be well within the experimental error bars. At higher fields the discontinuity at this wave vector becomes apparent (see Sec. III B 2). The gap in the $\boldsymbol{Q}_{\pi,\pi}$ branch, $\Delta_{\pi,\pi}=\mathcal{E}_0=0.172$ meV, is also in very good agreement with the INS measurements. Entire dispersion branches calculated numerically using the technique described above are shown in Fig. 10(b). They can be also seen as solid lines in Fig. 5 and apparently are in very good agreement with experimental data.

4. Spin-wave spectrum in the spin-flop phase

As we have already mentioned, we presently do not have theoretical results for the spin-wave dispersion in the presence of an external magnetic field. However, we can make some predictions for the spin-wave spectrum in the spin-flop phase (i.e., for $H>H_c$). After some tedious calculations that are omitted here, but are very similar to those performed in Sec. IV B 2, one arrives at the result that the contribution of the Dzyaloshinskii-Moriya term for the x (y) bonds is proportional to $\sin k_x$ ($\sin k_y$) and therefore *exactly* vanishes at the AFM zone center. In order to calculate the additional energy gap Δ_c in the spin-flop phase we thus need to consider only the KSEA terms. At $\boldsymbol{Q}=\boldsymbol{Q}_{\pi,\pi}$ (long-wavelength limit) the effect of KSEA interactions is identical to that of conventional easy-plane exchange anisotropy. The spectrum of a Heisenberg AFM with such anisotropy in a magnetic field is well known.[26] Both field and anisotropy split the twofold degenerate magnons in a Heisenberg system to give a gapless mode with linear dispersion and an ''optical'' mode with the energy gap at $\boldsymbol{Q}_{\pi,\pi}$ given by

$$\hbar\omega(\boldsymbol{Q}_{\pi,\pi})=\sqrt{\Delta_c^2+(g\mu_B H)^2},$$

$$\Delta_c=2\sqrt{2}JS\sqrt{2\delta}=2\sqrt{2}DS.$$

Substituting the known numerical values into this formula we obtain $\Delta_c=0.24$ meV, which is in reasonable agreement with the experimental result $\Delta_c=0.28$ meV.

V. DISCUSSION

We see that both the static and dynamic properties of $Ba_2CuGe_2O_7$ are quantitatively consistent with the presence of KSEA interactions. To be more precise, the experimental data unambiguously indicate the presence of an easy-plane anisotropy of exactly the same strength as predicted by the KSEA mechanism. It is important to stress that in a *slowly* rotating helix it is impossible to distinguish experimentally between single-ion easy-plane anisotropy of type $\Sigma_{n,m}(S^z_{n,m})^2/2$, two-ion anisotropy $(\Sigma_{n,m}[S^z_{n,m}S^z_{n+1,m}+S^z_{n,m}S^z_{n,m+1}]/2)$ or KSEA-type anisotropy $(\Sigma_{n,m}[S^y_{n,m}S^y_{n+1,m}+S^x_{n,m}S^x_{n,m+1}])$ of the same strength. Indeed, the difference between a pair of easy axes (KSEA term) and an easy plane (conventional single-ion or two-ion anisotropy) becomes apparent only when the period of the structure is comparable to the nearest-neighbor spin-spin separation, i.e., is only manifested in lattice effects. Alternatively, it can be observed in strong magnetic fields when the canting of spins towards the field direction becomes substantial. In $Ba_2CuGe_2O_7$, where the magnetic structure has a rather long periodicity, and where even at the critical field the uniform magnetization (spin canting) is small, these effects are expected to be insignificant. It is entirely possible that the weak ''quadrupolar'' in-plane anisotropy seen in horizontal-field experiments[15] is in fact such a lattice effect. Note that its strength is extremely small, of the order of 7×10^{-9} eV, and yet it can be reliably measured in a diffraction experiment where a magnetic field is applied in the (ab) crystallographic plane at different angles to the a axis.[15] Another possible manifestation of lattice effects is the intermediate phase seen just before the commensurate-incommensurate transition in a magnetic field applied along the c crystallographic axis.[14] A further study of these phenomena that distinguish between KSEA and other types of anisotropy in $Ba_2CuGe_2O_7$ is an interesting topic for future experimental and theoretical work.

One final comment has to be made in reference to another possible player in the spin Hamiltonian for $Ba_2CuGe_2O_7$: dipolar interactions. In principle, the ever-present dipolar term can and will influence both the ground-state spin configuration and the spin-wave spectrum in $Ba_2CuGe_2O_7$. Its effect, however, is expected to be insignificant compared even to the weakest terms that we have considered in our treatment. Indeed, nearest-neighbor spins in $Ba_2CuGe_2O_7$ are separated by $\Lambda=a/\sqrt{2}\approx6$ Å. For two nearest-neighbor spins the energy of dipolar coupling is of the order of $(g\mu_B)^2/\Lambda^3\approx1$ μeV. This is an order of magnitude less than the smallest energy scale in our model, which is the strength of KSEA anisotropy $J\alpha^2/2\approx15$ μeV. Moreover, in an almost-antiferromagnetic structure long-range dipolar interactions will be heavily suppressed by the sign alternation in the contribution of individual pairs of interacting spins. Our neglecting dipolar interactions in all the derivations above is thus justified.

In summary we have demonstrated that KSEA interactions can result in very interesting measurable effects, and

that no *additional* anisotropy is needed to reproduce the behavior observed in $Ba_2CuGe_2O_7$.

ACKNOWLEDGMENTS

This study was supported in part by NEDO (New Energy and Industrial Technology Development Organization) International Joint Research Grant and the U.S.-Japan Cooperative Program on Neutron Scattering. Work at BNL was carried out under Contract No. DE-AC02-98CH10886, Division of Material Science, U.S. Department of Energy. Experiments at NIST were partially supported by the NSF under Contract No. DMR-9413101.

*Also at Department of Physics and Astronomy, Johns Hopkins University, MD 21218 and P. L. Kapitza Institute for Physical Problems, Moscow, Russia.

[1] A. Zheludev *et al.*, Phys. Rev. B **54**, 15 163 (1996); Physica B **234-236**, 546 (1997).

[2] A. Zheludev *et al.*, Physica B **234-236**, 546 (1997).

[3] J. Jensen and A. R. Mackintosh, *Rare Earth Magnetism: Structures and Excitations* (Clarendon, Oxford, 1975).

[4] I. Dzyaloshinskii, Sov. Phys. JETP **5**, 1259 (1957).

[5] T. Moriya, Phys. Rev. **120**, 91 (1960).

[6] A. Yoshimori, J. Phys. Soc. Jpn. **14**, 807 (1959).

[7] P. Day and K. R. A. Ziebeck, J. Phys. C **13**, L01 (1980).

[8] A. Adam *et al.*, Solid State Commun. **35**, 1 (1980).

[9] Y. Ishikawa, K. Tajima, D. Bloch, and M. Roth, Solid State Commun. **19**, 525 (1976).

[10] Y. Ishikawa and M. Arai, J. Phys. Soc. Jpn. **53**, 2726 (1984).

[11] B. Lebech, J. Bernhard, and T. Flertoft, J. Phys.: Condens. Matter **1**, 6105 (1989).

[12] I. E. Dzyaloshinskii, J. Exp. Theor. Phys. **46**, 1420 (1964).

[13] A. Zheludev *et al.*, Phys. Rev. Lett. **78**, 4857 (1997).

[14] A. Zheludev *et al.*, Phys. Rev. B **57**, 2968 (1998).

[15] A. Zheludev *et al.*, Phys. Rev. B **56**, 14 006 (1997).

[16] In Ref. 1 we used a different notation for the exchange constant J, assuming the maximum exchange energy *per bond* is $2J$. In the present paper the exchange energy for every bond is counted only once in the Hamiltonian.

[17] T. A. Kaplan, Z. Phys. B **49**, 313 (1983).

[18] L. Shekhtman, O. Entin-Wohlman, and A. Aharony, Phys. Rev. Lett. **69**, 836 (1992).

[19] L. Shekhtman, A. Aharony, and O. Entin-Wohlman, Phys. Rev. B **47**, 174 (1993).

[20] A. Zheludev, S. Maslov, I. Tsukada, I. Zaliznyakj, L.-P. Regnault, T. Masuda, K. Uchinokura, R. Erwin, and G. Shirane, Phys. Rev. Lett. **81**, 5410 (1998).

[21] Y. Sasago (unpublished).

[22] P. W. Anderson, Phys. Rev. **115**, 2 (1959).

[23] T. Yildirim, A. B. Harris, A. Aharony, and O. Entin-Wohlman, Phys. Rev. B **52**, 10 239 (1995).

[24] I. A. Zaliznyak and M. E. Zhitomirsky, JETP **81**, 579 (1995).

[25] M. E. Zhitomirsky and I. A. Zaliznyak, Phys. Rev. B **53**, 3428 (1996).

[26] A. I. Akhiezer, V. G. Bar'yakhtar, and S. V. Peletminskii, *Spin Waves* (North-Holland, Amsterdam, 1968).